

Spin Distribution in Low-Spin (*meso*-Tetraalkylporphyrinato)iron(III) Complexes with $(d_{xz}, d_{yz})^4(d_{xy})^1$ Configuration. Studies by ^1H NMR, ^{13}C NMR, and EPR Spectroscopies

Takahisa Ikeue,^{†,‡} Yoshiki Ohgo,[†] Takashi Saitoh,^{||} Mikio Nakamura,^{*,†,||} Hiroshi Fujii,[⊥] and Masataka Yokoyama[§]

Contribution from the Department of Chemistry, Toho University School of Medicine, Ota-ku, Tokyo 143-8540, Japan, Division of Biomolecular Science, Graduate School of Science, Toho University, Funabashi 274-8510, Japan, Institute for Molecular Science, Okazaki 444-8585, Japan, and Department of Chemistry, Faculty of Science, Chiba University, Chiba 263-8522, Japan

Received June 28, 1999. Revised Manuscript Received February 3, 2000

Abstract: ^1H NMR, ^{13}C NMR, and EPR studies of a series of low-spin (*meso*-tetraalkylporphyrinato)iron(III) complexes, $[\text{Fe}(\text{TRP})(\text{L})_2]\text{X}$ where R = ^nPr , ^oPr , and ^iPr and L represents axial ligands such as imidazoles, pyridines, and cyanide, have revealed that the ground-state electron configuration of $[\text{Fe}(\text{T}^n\text{PrP})(\text{L})_2]\text{X}$ and $[\text{Fe}(\text{T}^o\text{PrP})(\text{L})_2]\text{X}$ is presented either as the common $(d_{xy})^2(d_{xz}, d_{yz})^3$ or as the less common $(d_{xz}, d_{yz})^4(d_{xy})^1$ depending on the axial ligands. The ground-state electron configuration of the isopropyl complexes $[\text{Fe}(\text{T}^i\text{PrP})(\text{L})_2]\text{X}$ is, however, presented as $(d_{xz}, d_{yz})^4(d_{xy})^1$ regardless of the kind of axial ligands. In every case, the contribution of the $(d_{xz}, d_{yz})^4(d_{xy})^1$ state to the electronic ground state increases in the following order: $\text{HIm} < 4\text{-Me}_2\text{NPy} < 2\text{-MeIm} < \text{CN}^- < 3\text{-MePy} < \text{Py} < 4\text{-CNPy}$. Combined analysis of the ^{13}C and ^1H NMR isotropic shifts together with the EPR g values have yielded the spin densities at the porphyrin carbon and nitrogen atoms. Estimated spin densities in $[\text{Fe}(\text{T}^i\text{PrP})(4\text{-CNPy})_2]^+$, which has the purest $(d_{xz}, d_{yz})^4(d_{xy})^1$ ground state among the complexes examined in this study, are as follows: *meso*-carbon, +0.045; α -pyrrole carbon, +0.0088; β -pyrrole carbon, -0.00026; and pyrrole nitrogen, +0.057. Thus, the relatively large spin densities are on the pyrrole nitrogen and *meso*-carbon atoms. The result is in sharp contrast to the spin distribution in the $(d_{xy})^2(d_{xz}, d_{yz})^3$ type complexes; the largest spin density is at the β -pyrrole carbon atoms in bis(1-methylimidazole)(*meso*-tetrphenylporphyrinato)iron(III), $[\text{Fe}(\text{TPP})(1\text{-MeIm})_2]^+$, as determined by Goff. The large downfield shift of the *meso*-carbon signal, $\delta +917.5$ ppm at -50 °C in $[\text{Fe}(\text{T}^i\text{PrP})(4\text{-CNPy})_2]^+$, is ascribed to the large spin densities at these carbon atoms. In contrast, the large upfield shift of the α -pyrrole carbon signal, $\delta -293.5$ ppm at the same temperature, is caused by the spin polarization from the adjacent *meso*-carbon and pyrrole nitrogen atoms.

Introduction

There are two types of electronic ground state in low-spin iron(III) porphyrin complexes. One is the commonly observed ground state with $(d_{xy})^2(d_{xz}, d_{yz})^3$ electron configuration and the other is the less common ground state with $(d_{xz}, d_{yz})^4(d_{xy})^1$ electron configuration.¹ Recent studies have revealed that the ground state of low-spin complexes is controlled by the nature of axial ligands.^{2–7} That is, the weak σ -donors stabilize the iron d_{π} orbitals, inducing the less common $(d_{xz}, d_{yz})^4(d_{xy})^1$ ground

state. Typical examples are $[\text{Fe}(\text{TPP})(^t\text{BuNC})_2]^+$ and $[\text{Fe}(\text{TMP})(4\text{-CNPy})_2]^+$.^{2,4,6,8} Complexes with a strongly S_4 -ruffled porphyrin core also adopt the $(d_{xz}, d_{yz})^4(d_{xy})^1$ ground state even if the axial ligands are strong bases such as CN^- and 2-MeIm.^{9–14}

* To whom correspondence should be addressed. mnakamu@med.toho-u.ac.jp.

[†] Current address: Department of Chemistry, Faculty of Science, Chiba University, Chiba, 263-8522, Japan.

[‡] Toho University School of Medicine.

^{||} Graduate School of Science, Toho University.

[⊥] Institute for Molecular Science.

[§] Chiba University.

(1) Walker, F. A.; Simonis, U. Proton NMR Spectroscopy of Model Hemes. In *NMR of Paramagnetic Molecules*; Berliner, L. J., Reuben, J., Eds.; Plenum Press: New York, 1993; Biological Magnetic Resonance, Vol. 12; pp 133–274.

(2) Safo, M. K.; Gupta, G. P.; Watson, C. T.; Simonis, U.; Walker, F. A.; Scheidt, W. R. *J. Am. Chem. Soc.* **1992**, *114*, 7066–7075.

(3) Safo, M. K.; Walker, F. A.; Raitsimring, A. M.; Walters, W. P.; Dolata, D. P.; Debrunner, P. G.; Scheidt, W. R. *J. Am. Chem. Soc.* **1994**, *116*, 7760–7770.

(4) Walker, F. A.; Nasri, H.; Turowska-Tyrk, I.; Mohanrao, K.; Watson, C. T.; Shokhirev, N. V.; Debrunner, P. G.; Scheidt, W. R. *J. Am. Chem. Soc.* **1996**, *118*, 12109–12118.

(5) Cheesman, M. R.; Walker, F. A. *J. Am. Chem. Soc.* **1996**, *118*, 7373–7380.

(6) Simonneaux, G.; Hindre, F.; Le Plouzennec, M. *Inorg. Chem.* **1989**, *28*, 823–825.

(7) Pilard, M.-A.; Guillemot, M.; Toupet, L.; Jordanov, J.; Simonneaux, G. *Inorg. Chem.* **1997**, *36*, 6307–6314.

(8) Abbreviations: TPP, TMP, and TRP, dianions of *meso*-tetrphenylporphyrin, *meso*-tetramesitylporphyrin, and *meso*-tetraalkylporphyrin, respectively; T^nPrP , T^oPrP , and T^iPrP , dianions of *meso*-tetrapropylporphyrin, *meso*-tetracyclopropylporphyrin, and *meso*-tetraisopropylporphyrin, respectively; HIm, limidazole; 2-MeIm, 2-methylimidazole; 4-Me₂NPy, 4-(*N,N*-dimethylamino)pyridine; Py, pyridine; 3-MePy, 3-methylpyridine; 4-CNPy, 4-cyanopyridine; $[\text{Fe}(\text{TRP})(\text{L})_2]\text{X}$, low spin-complexes of (*meso*-tetraalkylporphyrinato)iron(III) complexes where R = ^nPr , ^oPr , and ^iPr and L's are the seven ligands listed above.

(9) Nakamura, M.; Ikeue, T.; Neya, S.; Funasaki, N.; Nakamura, N. *Inorg. Chem.* **1996**, *35*, 3731–3732.

(10) Nakamura, M.; Ikeue, T.; Fujii, H.; Yoshimura, T. *J. Am. Chem. Soc.* **1997**, *119*, 6284–6291.

(11) Nakamura, M.; Ikeue, T.; Fujii, H.; Yoshimura, T.; Tajima, K. *Inorg. Chem.* **1998**, *37*, 2405–2414.

Examples are $[\text{Fe}(\text{T}^i\text{PrP})(\text{CN})_2]^-$ and $[\text{Fe}(\text{T}^i\text{PrP})(2\text{-MeIm})_2]^+$.^{10,11} The S_4 -ruffling of the porphyrin core would weaken the p_π -iron)- $3e_g$ (porphyrin) interaction¹⁰ and strengthen the d_{xy} (iron)- a_{2u} (porphyrin) interaction.^{3,4,10} The former stabilizes the iron d_π orbitals and the latter destabilizes the d_{xy} orbital, resulting in the stabilization of the $(d_{xz}, d_{yz})^4(d_{xy})^1$ state relative to the $(d_{xy})^2(d_{xz}, d_{yz})^3$ state.

Recent studies have also revealed that the difference in electron configuration induces fairly large changes in spectroscopic properties such as NMR chemical shift values, EPR g values, Mössbauer ΔE_q values, MCD band intensities, etc.^{2-7,9-15} For example, the complexes with $(d_{xz}, d_{yz})^4(d_{xy})^1$ ground state generally show the downfield shifted pyrrole signals in ^1H NMR spectra; the chemical shift of the pyrrole protons in $[\text{Fe}(\text{T}^i\text{PrP})(\text{CN})_2]^-$ is +11.9 ppm at -25°C as compared with -22.6 ppm in $[\text{Fe}(\text{TPP})(1\text{-MeIm})_2]^+$ which has the common $(d_{xy})^2(d_{xz}, d_{yz})^3$ ground state.^{10,16} Similarly, meso-carbon signals appear downfield in the $(d_{xz}, d_{yz})^4(d_{xy})^1$ type complexes as compared with those in the $(d_{xy})^2(d_{xz}, d_{yz})^3$ type complexes; the chemical shifts of the meso carbons in $[\text{Fe}(\text{T}^i\text{PrP})(2\text{-MeIm})_2]^+$ and $[\text{Fe}(\text{TPP})(1\text{-MeIm})_2]^+$ are 452.0 and 25.6 ppm at -60°C , respectively.^{11,16} These results clearly indicate that the spin distribution at the porphyrin carbon and nitrogen atoms is quite different between two types of complexes. Although the spin distribution in low-spin iron(III) porphyrin complexes has been extensively studied by Wüthrich, La Mar, Goff, and others, all of the complexes examined so far have the common ground state $(d_{xy})^2(d_{xz}, d_{yz})^3$ electron configuration.¹⁷⁻²⁰ To determine how the unpaired electron spin density is distributed within the porphyrin macrocycle of complexes with the less common ground-state configuration $(d_{xz}, d_{yz})^4(d_{xy})^1$, we have examined the ^1H NMR, ^{13}C NMR, and EPR spectra of a large number of low-spin (meso-tetraalkylporphyrinato)iron(III) complexes, $[\text{Fe}(\text{T}^i\text{PrP})(\text{L})_2]\text{X}$, $[\text{Fe}(\text{T}^o\text{PrP})(\text{L})_2]\text{X}$, and $[\text{Fe}(\text{T}^i\text{PrP})(\text{L})_2]\text{X}$, carrying various axial ligands such as imidazole, 2-methylimidazole, 4-(*N,N*-dimethylamino)pyridine, 3-methylpyridine, pyridine, 4-cyanopyridine, and cyanide. In this paper, we report the spin densities at porphyrin carbon and nitrogen atoms together with some characteristic features of the ^{13}C NMR chemical shifts in the complexes with the less common $(d_{xz}, d_{yz})^4(d_{xy})^1$ ground state.

Experimental Section

Synthesis of Free Base Porphyrins, (TRP) $_2$ (R = ^nPr , ^oPr , ^iPr). $(\text{T}^i\text{PrP})\text{H}_2$ was prepared according to Neya's method.^{21,22} $(\text{T}^o\text{PrP})\text{H}_2$ was prepared according to Lindsey's method.²³

(i) meso-Tetracyclopropylporphyrin, (T o PrP) $_2$: A propionic acid (20 mL) solution of cyclopropanecarboxaldehyde (0.70 g, 10 mmol) and pyrrole (0.67 g, 10 mmol) was refluxed for 2 h at 100°C . After the solution was cooled, the reaction mixture was treated with aqueous

NaOH. The organic products were extracted with CH_2Cl_2 and then purified by column chromatography on alumina. Elution with dichloromethane yielded a pure material as a purple solid. FAB-HRMS (m/z): $[\text{M} + \text{H}]^+$ calcd for $\text{C}_{32}\text{H}_{31}\text{N}_4$, 471.2549; found, 471.2549 (base peak). ^1H NMR (CDCl_3 , 25°C): δ -2.40 (2H, NH), 1.41 (8H, meso- β -H), 1.81 (8H, meso- β -H), 4.20 (4H, meso- α -H), 9.72 (8H, py-H).

(ii) meso-Tetracyclopropylporphyrin (pyrrole- d_8), (T o PrP) $_2$ -(pyrrole- d_8): This compound was prepared similarly from pyrrole (0.67 g, 10 mmol) and cyclopropanecarboxaldehyde (0.70 g, 10 mmol) in refluxing propionic acid- d_1 (99 atom % D, 20 mL) solution. The ^1H NMR spectrum has revealed that ca. 60% of pyrrole β -hydrogen was replaced by deuterium.

Synthesis of High-Spin Complexes, [Fe(TRP)Cl] (R = ^nPr , ^oPr , ^iPr). **(i) [Fe(T o PrP)Cl]:** A methanol-chloroform (1:3) solution of $(\text{T}^o\text{PrP})\text{H}_2$ was refluxed for 6 h in the presence of excess $\text{FeCl}_2 \cdot 4\text{H}_2\text{O}$. After the reaction, the solvents were removed and the resultant oily material was purified by column chromatography on silica gel using CH_2Cl_2 - CH_3OH as eluents. The fractions containing iron(III) porphyrin complexes were then treated with 1.0 N aqueous HCl. The organic layer was separated and dried over sodium sulfate. After the evaporation of the solvent, $[\text{Fe}(\text{T}^o\text{PrP})\text{Cl}]$ was recrystallized from CH_2Cl_2 -hexane. ^1H NMR (CD_2Cl_2 , 25°C): δ 1.29 (8H, meso- β -H), 2.95 (12H, meso- γ -H), 62.9 (8H, meso- α -H), 87.7 (8H, pyrrole-H).

(ii) [Fe(T i PrP)Cl]: Insertion of iron into $(\text{T}^i\text{PrP})\text{H}_2$ was carried out using $\text{FeCl}_2 \cdot 4\text{H}_2\text{O}$ in refluxing methanol-chloroform (1:3) solution. After the reaction, the solvents were removed and the resultant oily material was purified by column chromatography on silica gel using CH_2Cl_2 and CH_3OH as eluents. The fractions containing iron(III) porphyrin complexes were then treated with 1.0 N aqueous HCl. The organic layer was separated and dried over sodium sulfate. After the evaporation of the solvent, $[\text{Fe}(\text{T}^i\text{PrP})\text{Cl}]$ was recrystallized from CH_2Cl_2 -hexane. ^1H NMR (CD_2Cl_2 , 25°C): δ 0.12 (8H, meso- β -H), 0.46 (8H, meso- β -H), 85.1 (8H, py-H), 164.2 (4H, meso- α -H).

(iii) [Fe(T i PrP)Cl]: Insertion of iron into $(\text{T}^i\text{PrP})\text{H}_2$ was carried out using $\text{FeCl}_2 \cdot 4\text{H}_2\text{O}$ in refluxing methanol-chloroform (1:3) solution. $[\text{Fe}(\text{T}^i\text{PrP})\text{Cl}]$ was isolated and purified similarly as $[\text{Fe}(\text{T}^o\text{PrP})\text{Cl}]$.¹⁰

Synthesis of Low-Spin Complexes, [Fe(TRP)(L) $_2$]X. The CD_2Cl_2 solution of high-spin $[\text{Fe}(\text{TRP})\text{Cl}]$ placed in an NMR sample tube was treated with 4 to 6 equiv of HIm, 2-MeIm, 4-NMe $_2$ Py, and NBu_4CN . In each case, complete conversion from the high-spin $[\text{Fe}(\text{TRP})\text{Cl}]$ to the low-spin $[\text{Fe}(\text{TRP})(\text{X})_2]\text{X}$ was confirmed by the ^1H NMR spectra. The conversion was, however, incomplete in the case of 3-MePy, Py, and 4-CNPy. Thus, the perchlorate complexes $[\text{Fe}(\text{TRP})(\text{THF})_2]\text{ClO}_4$, prepared by the treatment of $[\text{Fe}(\text{TRP})\text{Cl}]$ with the THF solution of AgClO_4 ,²⁴ were used instead of $[\text{Fe}(\text{TRP})\text{Cl}]$ for the preparation of the bis(Py), bis(3-MePy), and bis(4-CNPy) complexes.

Synthesis of 2-MeIm- d_5 . Deuterium exchange reaction was carried out according to the literature.²⁵ 2-MeIm (250 mg) in D_2O (99 atom % D, 7 mL) was heated at 250°C in a sealed glass tube for 6 h. The reaction mixture was cooled and the solution was evaporated to dryness. The resulting residue was recrystallized from benzene and then sublimed. ^1H NMR analysis revealed that the extent of deuteration was ca. 98%.

Physical Measurement. ^1H and ^{13}C NMR spectra were recorded on a JEOL LA300 spectrometer operating at 300.4 MHz for proton. Chemical shifts were referenced to the residual peaks of the CD_2Cl_2 (δ 5.32 ppm for ^1H and 53.1 ppm for ^{13}C). Proton homonuclear COSY spectra were collected after the measurement of the standard 1D reference spectra. The 2D COSY spectra were collected by use of 1024 points in t_2 over the bandwidth of 8.4 kHz with 512 t_1 blocks and 128 scans per block in which 4 dummy scans were included. UV-visible spectra were recorded on a Hitachi 200-10 spectrophotometer at 25°C with CH_2Cl_2 as solvent. Mass spectra were recorded on a JEOL JMS-HX 110 mass spectrometer. For high-resolution fast-atom-bombardment mass spectra (FAB-HRMS), *m*-nitrobenzyl alcohol was used for the matrix formation. EPR spectra were measured at 4.2 K with a Bruker ESP-300E spectrometer operating at X band and equipped with an

(12) Wolowiec, S.; Latos-Grazynski, L.; Mazzanti, M.; Marchon, J.-C. *Inorg. Chem.* **1997**, *36*, 5761-5771.

(13) Wojaczynski, J.; Latos-Grazynski, L.; Glowiak, T. *Inorg. Chem.* **1997**, *36*, 6299-6306.

(14) Wolowiec, S.; Latos-Grazynski, L.; Toronto, D.; Marchon, J.-C. *Inorg. Chem.* **1998**, *37*, 724-732.

(15) Geze, C.; Legrand, N.; Bondon, A.; Simonneaux, G. *Inorg. Chim. Acta* **1992**, *195*, 73-76.

(16) Nakamura, M.; Tajima, K.; Tada, K.; Ishizu, K.; Nakamura, N. *Inorg. Chim. Acta* **1994**, *224*, 113-124.

(17) Wüthrich, K.; Baumann, R. *Helv. Chim. Acta* **1973**, *56*, 585-596.

(18) Wüthrich, K.; Baumann, R. *Helv. Chim. Acta* **1974**, *57*, 336-350.

(19) La Mar, G. N.; Viscio, D. B.; Smith, K. M.; Caughey, W. S.; Smith, M. L. *J. Am. Chem. Soc.* **1978**, *100*, 8085-8092.

(20) Goff, H. M. *J. Am. Chem. Soc.* **1981**, *103*, 3714-3722.

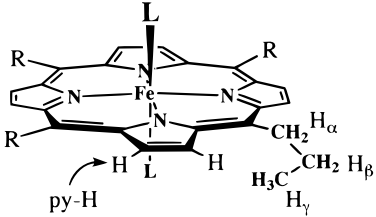
(21) Neya, S.; Yodo, H.; Funasaki, N. *J. Heterocycl. Chem.* **1993**, *30*, 549-550.

(22) Neya, S.; Funasaki, N. *J. Heterocycl. Chem.* **1997**, *34*, 689-690.

(23) Wagner, R. W.; Lawrence, D. S.; Lindsey, J. S. *Tetrahedron, Lett.* **1987**, *28*, 3069-3070.

(24) Ogoshi, H.; Sugimoto, H.; Watanabe, E.; Yoshida, Z.; Maeda, Y.; Sakai, H. *Bull. Chem. Soc. Jpn.* **1981**, *54*, 3414-3419.

(25) Stein, K. P.; Spiro, T. G. *Proc. Natl. Acad. Sci. U.S.A.* **1979**, *76*, 549-552.

Table 1. ^1H NMR Chemical Shifts of $[\text{Fe}(\text{TRP})(\text{L})_2]^*$ ($\text{R} = {}^n\text{Pr}$, ${}^c\text{Pr}$, or ${}^i\text{Pr}$; * = + or -) Taken in CD_2Cl_2 at $-50\text{ }^\circ\text{C}$


$[\text{Fe}(\text{TRP})(\text{L})_2]^*$						
R	L	H_α	H_β	H_γ	py-H	
${}^n\text{Pr}$	HIm	1.72	-1.47	-0.46	-21.45	
	4-NMe ₂ Py	9.73	-0.92	-0.43	-16.68	
	2-MeIm ^a	21.30	0.79	-0.01	-8.20	
	CN ⁻	30.91	0.09	0.82	-3.48	
	3-MePy	51.36	1.77	-0.87	4.49	
	Py	57.92	1.65	-1.27	7.07	
${}^c\text{Pr}$	4-CNPY	88.52	0.68	-0.20	13.03	
	HIm	10.88	-1.52	-2.26	-	-18.70
	4-NMe ₂ Py	26.37	-1.21	-2.81	-	-14.31
	2-MeIm	35.48	-9.29	<i>b</i>	-	-12.27
		51.32	-6.50	-	-	-9.98
			-3.28	-	-	-7.25
		-2.06	-	-	-4.46	
${}^i\text{Pr}$	CN ⁻	91.87	-0.15	-1.82	-	4.28
	3-MePy	115.25	-0.27	-3.35	-	7.25
	Py	121.35	-0.35	-3.93	-	8.39
	4-CNPY	189.49	-1.56	-4.16	-	14.89
${}^i\text{Pr}$	HIm	16.14	3.91	-	0.11	
	4-NMe ₂ Py	19.79	4.78	-	4.00	
		23.09	3.47	-	4.12	
			6.51	-	7.50	
			7.51	-	8.15	
	CN ⁻	28.68	6.67	-	12.26	
	3-MePy	33.20	7.76	-	14.66	
	Py	33.95	7.83	-	14.94	
	4-CNPY	41.63	8.87	-	15.62	

^a Extrapolated values from high temperature. At $-50\text{ }^\circ\text{C}$, every signal becomes too broad to detect due to the rotation of 2-MeIm ligand.
^b Some signals are still too broad to detect.

Oxford helium cryostat. The samples for the EPR measurement were prepared by the addition of 4 to 6 equiv of the ligands into the CH_2Cl_2 solutions of $[\text{Fe}(\text{TRP})\text{Cl}]$ or $[\text{Fe}(\text{TRP})\text{ClO}_4]$. The concentration of EPR samples was 5–8 mM. The observed EPR spectra had enough quality to determine their g values from the spectra except for some broad signals. To determine g values of the spectra exactly, the observed EPR spectra were simulated by the Bruker WIN-EPR Sim Fonia program using Gaussian line function and the following parameters: data points, 500; θ division, 500; ψ division, 90.

Results

^1H NMR Spectra. Table 1 shows the ^1H NMR chemical shifts of the pyrrole and meso alkyl protons in a series of low-spin complexes $[\text{Fe}({}^n\text{PrP})(\text{L})_2]\text{X}$, $[\text{Fe}({}^c\text{PrP})(\text{CN})_2]\text{X}$, and $[\text{Fe}({}^i\text{PrP})(\text{L})_2]\text{X}$ taken at $-50\text{ }^\circ\text{C}$ together with the labeling of the proton atoms for $[\text{Fe}({}^n\text{PrP})(\text{L})_2]\text{X}$. Proton atoms of the other complexes are similarly labeled. Signal assignment of the pyrrole and alkyl protons was unambiguously done on the basis of the relative integral intensities, temperature dependence of each signal, and spectral comparison with the corresponding deuterated complexes. Chemical shifts of all the protons including those of the ligand protons taken at various temperatures are listed in Tables S1–S3 of the Supporting Information though ambiguity still remains in the assignment of some protons of the coordinated imidazole ligands. Curie plots of the pyrrole

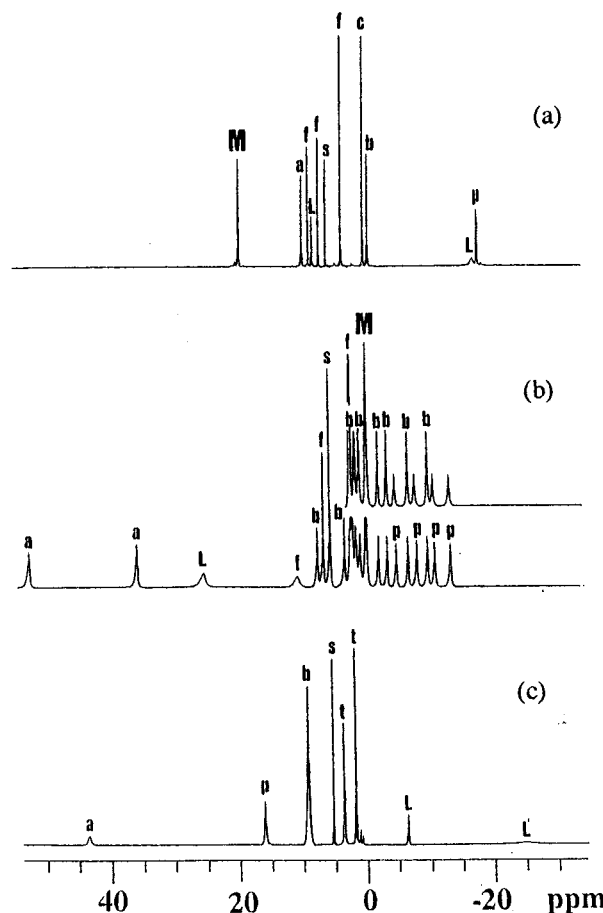
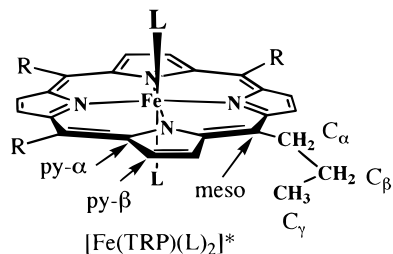


Figure 1. ^1H NMR spectra of (a) $[\text{Fe}({}^n\text{PrP})(4\text{-Me}_2\text{NPY})_2]^+$, (b) $[\text{Fe}({}^c\text{PrP})(2\text{-MeIm})_2]^+$, and (c) $[\text{Fe}({}^i\text{PrP})(4\text{-CNPY})_2]^+$ taken in CD_2Cl_2 solution at $-60\text{ }^\circ\text{C}$. Part of the spectrum of pyrrole deuterated $[\text{Fe}({}^c\text{PrP})(2\text{-MeIm})_2]^+$ is given in the inset of part b. Signal assignment: (a, b, and c) α -, β -, and γ -protons of the meso alkyl groups, respectively; (p) pyrrole-H; (L) coordinated ligand; (M) ligand methyl; (f) free ligand; (t) THF; (s) solvent.

proton signals of $[\text{Fe}({}^n\text{PrP})(\text{L})_2]\text{X}$, $[\text{Fe}({}^c\text{PrP})(\text{CN})_2]\text{X}$, and $[\text{Fe}({}^i\text{PrP})(\text{L})_2]\text{X}$ are shown in Figures S1, S2, and S3, respectively. Table 1 lists the chemical shift positions of the pyrrole protons in order of increasing shifts. The order given below is the same regardless of the difference in the meso alkyl groups; HIm < 4-Me₂NPy < 2-MeIm < CN < 3-MePy < Py < 4-CNPY. It should be noted that the chemical shifts of the meso α -protons (H_α) also follow this order. Figure 1 shows the ^1H NMR spectra of $[\text{Fe}({}^n\text{PrP})(4\text{-NMe}_2\text{Py})_2]^+$, $[\text{Fe}({}^c\text{PrP})(2\text{-MeIm})_2]^+$, and $[\text{Fe}({}^i\text{PrP})(4\text{-CNPY})_2]^+$ taken at $-60\text{ }^\circ\text{C}$ as typical examples. As shown in Figure 1b, $[\text{Fe}({}^c\text{PrP})(2\text{-MeIm})_2]^+$ gave a very complicated spectrum due to the slow rotation of the coordinated 2-MeIm ligands on the ^1H NMR time scale.^{9,12} The meso β -protons (H_β) gave two signals at 25 $^\circ\text{C}$, each of which split into four signals at lower temperature. The pyrrole signal also split into four signals as the temperature was lowered. Assignment of the pyrrole signals in $[\text{Fe}({}^c\text{PrP})(2\text{-MeIm})_2]\text{Cl}$ was carried out by the spectral comparison with $[\text{Fe}({}^c\text{PrP})(2\text{-MeIm})_2]\text{Cl}(\text{pyrrole-}d_8)$ and $[\text{Fe}({}^c\text{PrP})(2\text{-MeIm-}d_5)_2]\text{Cl}$; a part of the spectrum of $[\text{Fe}({}^c\text{PrP})(2\text{-MeIm})_2]\text{Cl}(\text{pyrrole-}d_8)$ is given in the insets of Figure 1b. The proton homonuclear COSY spectra were also helpful to assign the meso β -protons (H_β), which is given in Figure S4 of the Supporting Information.

^{13}C NMR Spectra. Table 2 shows the ^{13}C NMR chemical shifts of the pyrrole and meso alkyl carbons in a series of low-

Table 2. ^{13}C NMR Chemical Shifts of $[\text{Fe}(\text{TRP})(\text{L})_2]^*$ (R = ^nPr , ^cPr , or ^iPr ; * = + or -) Taken in CD_2Cl_2 at -50°C



R	L	meso	C_α	C_β	C_γ	py- α	py- β
^nPr	HIm	73.1	14.5	64.5	12.4	0.0	73.6
	4-NMe ₂ Py	130.5	-7.3	108.6	12.6	-2.2	84.3
	2-MeIm ^a	<i>a</i>	<i>a</i>	<i>a</i>	<i>a</i>	<i>a</i>	<i>a</i>
	CN ⁻	336.1	-56.6	249.7	17.9	-72.7	61.2
	3-MePy	470.0	-120.6	348.8	16.9	-88.5	77.0
	Py	526.5	-140.6	385.7	17.6	-108.2	74.3
	4-CNPy	814.7	-245.1	574.2	23.0	-262.7	66.0
^cPr	HIm	97.1	-6.2	17.5	-	11.8	79.6
	4-NMe ₂ Py	127.4	-25.4	29.7	-	8.5	88.0
	2-MeIm	149.1	<i>b</i>	<i>b</i>	-	-62.0	<i>b</i>
		231.6				-36.1	
						+37.7	
						+39.8	
						-84.2	61.2
^iPr	CN ⁻	386.7	-98.9	91.4	-	-71.1	79.6
	3-MePy	431.6	-133.0	102.8	-	-81.3	78.7
	Py	448.9	-141.5	106.8	-	-211.9	71.7
	4-CNPy	680.1	-240.8	155.9	-		
	HIm	331.6	-55.3	172.5	-	-28.3	76.5
	4-NMe ₂ Py	402.2	76.6	207.3	-	-47.2	81.1
	2-MeIm	379.2	-65.4	<i>b</i>	-	-28.1	65.6
	488.7	-104.2		-	-34.3	67.6	
					-93.4	80.4	
					-123.7	85.4	
					-186.0	54.7	
					-165.2	71.6	
					-179.3	71.4	
					-293.5	74.8	

^a Measurement was difficult due to the low solubility. ^b Signals are too broad to detect due to the rotation of 2-MeIm ligand.

spin complexes $[\text{Fe}(\text{T}^n\text{PrP})(\text{L})_2]\text{X}$, $[\text{Fe}(\text{T}^c\text{PrP})(\text{CN})_2]\text{X}$, and $[\text{Fe}(\text{T}^i\text{PrP})(\text{L})_2]\text{X}$ taken at -50°C together with the labeling of the carbon atoms for $[\text{Fe}(\text{T}^n\text{PrP})(\text{L})_2]\text{X}$. Carbon atoms of the other complexes are similarly labeled. The porphyrin carbon signals were assigned on the basis of the acquisition of proton-coupled ^{13}C NMR spectra. Chemical shifts of all the carbon atoms including those of the ligand carbons taken at various temperatures are listed in Tables S4–S6 of the Supporting Information though ambiguity still remains in the assignment of some ligand signals. In Table 2, the axial ligands are listed in the same order as that in Table 1. Nevertheless, the meso carbon signals showed downfield shift in this order regardless of the kind of meso alkyl groups. The difference in chemical shifts of the meso carbon atoms was fairly large among the complexes, ranging from 73.1 ppm in $[\text{Fe}(\text{T}^n\text{PrP})(\text{HIm})_2]^+$ to 917.5 ppm in $[\text{Fe}(\text{T}^i\text{PrP})(4\text{-CNPy})_2]^+$. Other signals such as meso α - and β -carbon (C_α , C_β) and α -pyrrole carbon (py- α) signals moved upfield or downfield in the same order. Only the β -pyrrole carbon (py- β) signals were observed in a relatively narrow range of 54.7–88.0 ppm. Figure 2 shows the ^{13}C NMR spectra of $[\text{Fe}(\text{T}^n\text{PrP})(4\text{-NMe}_2\text{Py})_2]^+$, $[\text{Fe}(\text{T}^c\text{PrP})(2\text{-MeIm})_2]^+$, and $[\text{Fe}(\text{T}^i\text{PrP})(4\text{-CNPy})_2]^+$ taken at 25°C as typical examples. Although the ligand signals in $[\text{Fe}(\text{T}^n\text{PrP})(4\text{-NMe}_2\text{Py})_2]^+$ appeared at 24.5, 42.5, 133.2, and 164.5 ppm, those in $[\text{Fe}(\text{T}^c\text{PrP})(2\text{-MeIm})_2]^+$ and $[\text{Fe}(\text{T}^i\text{PrP})(4\text{-CNPy})_2]^+$ could not be observed at this temperature due to the exchange broadening.

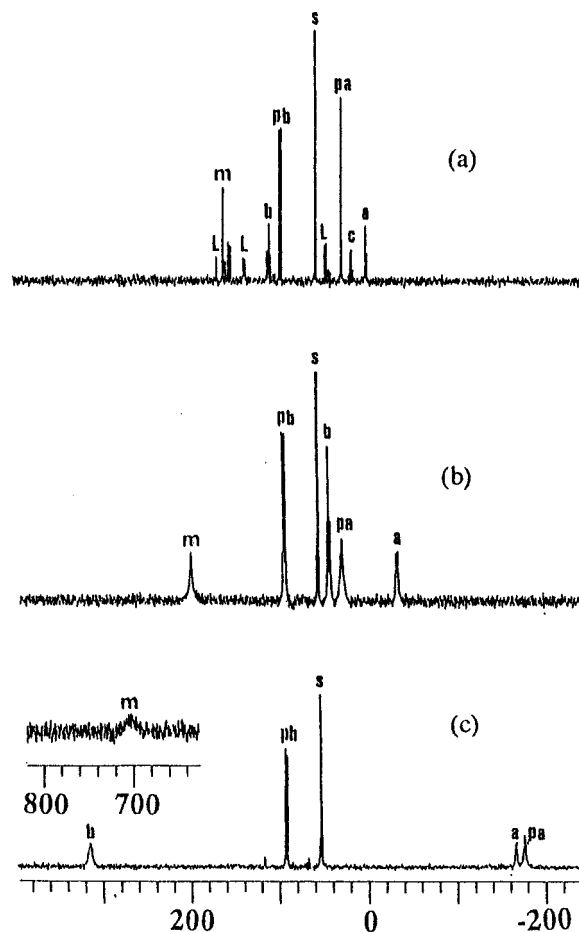


Figure 2. ^{13}C NMR spectra of (a) $[\text{Fe}(\text{T}^n\text{PrP})(4\text{-NMe}_2\text{Py})_2]^+$, (b) $[\text{Fe}(\text{T}^c\text{PrP})(2\text{-MeIm})_2]^+$, and (c) $[\text{Fe}(\text{T}^i\text{PrP})(4\text{-CNPy})_2]^+$ taken in CD_2Cl_2 solution at 25°C . Signal assignment: (a, b, and c) α -, β -, and γ -carbons of the meso alkyl groups, respectively; (m) meso; (pa and pb) α - and β -pyrrole carbons, respectively; (L) coordinated ligand; (s) CD_2Cl_2 .

EPR Spectra. Figure 3a demonstrates the EPR spectrum of $[\text{Fe}(\text{T}^i\text{PrP})(4\text{-CNPy})_2]^+$, which exhibits a good axial type spectrum. Complexes such as $[\text{Fe}(\text{T}^i\text{PrP})(\text{Py})_2]^+$, $[\text{Fe}(\text{T}^i\text{PrP})(\text{CN})_2]^-$, $[\text{Fe}(\text{T}^c\text{PrP})(4\text{-CNPy})_2]^+$, and $[\text{Fe}(\text{T}^n\text{PrP})(4\text{-CNPy})_2]^+$ showed similar spectra. In these complexes, the $g_\perp(g_1, g_2)$ and $g_\parallel(g_3)$ values, obtained directly from the observed spectra, coincided with those determined by the computer simulation. Figure 3b shows the EPR spectrum of $[\text{Fe}(\text{T}^c\text{PrP})(\text{Py})_2]^+$. Although the spectrum is classified as the axial type, the g_\parallel signal was not observed. Complexes such as $[\text{Fe}(\text{T}^i\text{PrP})(2\text{-MeIm})_2]^+$, $[\text{Fe}(\text{T}^i\text{PrP})(4\text{-Me}_2\text{NPy})_2]^+$, $[\text{Fe}(\text{T}^i\text{PrP})(\text{HIm})_2]^+$, $[\text{Fe}(\text{T}^c\text{PrP})(\text{Py})_2]^+$, $[\text{Fe}(\text{T}^c\text{PrP})(\text{CN})_2]^-$, $[\text{Fe}(\text{T}^n\text{PrP})(\text{Py})_2]^+$, and $[\text{Fe}(\text{T}^n\text{PrP})(\text{CN})_2]^-$ fall into this category. As shown in Figure 3c, $[\text{Fe}(\text{T}^i\text{PrP})(\text{HIm})_2]^+$ gave a rhombic type spectrum with much broader signals than those of $[\text{Fe}(\text{TPP})(\text{HIm})_2]^+$.^{26–29} Complexes such as $[\text{Fe}(\text{T}^c\text{PrP})(2\text{-MeIm})_2]^+$, $[\text{Fe}(\text{T}^c\text{PrP})(\text{HIm})_2]^+$, $[\text{Fe}(\text{T}^c\text{PrP})(4\text{-$

(26) Walker, F. A.; Reis, D.; Balke, V. L. *J. Am. Chem. Soc.* **1984**, *106*, 6888–6898.

(27) Walker, F. A.; Huynh, B. H.; Scheidt, W. R.; Osvath, S. R. *J. Am. Chem. Soc.* **1986**, *108*, 5288–5297.

(28) Hatano, K.; Safo, M. K.; Walker, F. A.; Scheidt, W. R. *Inorg. Chem.* **1991**, *30*, 1643–1650.

(29) Existence of several conformers caused by the difference in ligand orientation could be one of the reasons for the broad EPR spectrum; the spectrum could be broad if each conformer has slightly different g values. Another possible reason is the inhomogeneous broadening. In the EPR measurements, CH_2Cl_2 was used as a solvent since CD_2Cl_2 was used for the ^1H and ^{13}C NMR measurements. It is possible that we could not obtain a good glass in this solvent at 4.2 K .

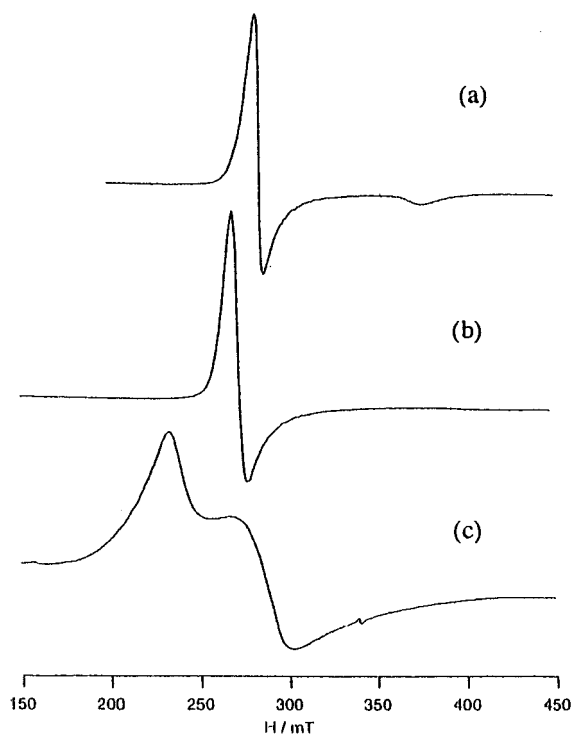


Figure 3. EPR spectra of (a) $[\text{Fe}(\text{T}^i\text{PrP})(4\text{-CNPY})_2]^+$, (b) $[\text{Fe}(\text{T}^c\text{PrP})(\text{Py})_2]^+$, and (c) $[\text{Fe}(\text{T}^n\text{PrP})(\text{HIm})_2]^+$ taken in frozen CH_2Cl_2 solution at 4.2 K.

Table 3. EPR g Values of $[\text{Fe}(\text{TRP})(\text{L})_2]^*$ ($\text{R} = {}^n\text{Pr}, {}^c\text{Pr}, \text{or } {}^i\text{Pr}$; $*$ = + or -) Taken in Frozen CHCl_2 Solution at 4.2 K

R	L	g_1	g_2	g_3	config ^d
ⁿ Pr	HIm	2.90	2.35	(1.45) ^c	d_{xy}
	4-NMe ₂ Py	3.10	2.10		d_{xy}
	2-MeIm ^a	2.85	2.10		d_{xy}
	CN ⁻	2.51	2.51		d_{xy}
	Py	2.55	2.55		d_{xy}
	4-CNPY	2.46	2.46	1.68	d_{xy}
^c Pr	HIm	2.87	2.42		d_{xy}
	4-NMe ₂ Py	3.10	2.00		d_{xy}
	2-MeIm ^a	2.90	2.10		d_{xy}
	CN ⁻	2.49	2.49		d_{xy}
	Py	2.56	2.56	(1.3) ^c	d_{xy}
	4-CNPY	2.49	2.49	1.58	d_{xy}
ⁱ Pr	HIm	2.55	2.55		d_{xy}
	4-NMe ₂ Py	2.54	2.54		d_{xy}
	2-MeIm ^a	2.58	2.58		d_{xy}
	CN ^{-b}	2.42	2.42	1.74	d_{xy}
	Py ^b	2.52	2.52	1.60	d_{xy}
	4-CNPY	2.41	2.41	1.79	d_{xy}

^a M. Nakamura et al.¹¹ ^b M. Nakamura et al.¹⁰ ^c Speculated value. ^d The d_{xy} and d_{xz} represent the ground state with $(d_{xy})^2(d_{xz}, d_{yz})^3$ and $(d_{xz}, d_{yz})^4(d_{xy})^1$ electron configuration, respectively.

$\text{Me}_2\text{NPy})_2]^+$, $[\text{Fe}(\text{T}^n\text{PrP})(2\text{-MeIm})_2]^+$, $[\text{Fe}(\text{T}^n\text{PrP})(4\text{-Me}_2\text{NPy})_2]^+$, and $[\text{Fe}(\text{T}^n\text{PrP})(\text{HIm})_2]^+$ exhibited similar spectra. The EPR g values of all the complexes examined in this study were determined by the computer simulation. They are listed in Table 3 in the decreasing order $g_1 > g_2 > g_3$.

Discussion

Electron Configuration. ¹H NMR chemical shift of the pyrrole protons is a good probe to determine the electronic ground state of the low-spin iron(III) porphyrin complexes.^{1-4,6,7,9-15} Complexes with $(d_{xz}, d_{yz})^4(d_{xy})^1$ ground state generally show pyrrole signals at $\delta > 0$ ppm at 25 °C in the tetraalkylporphyrin system.^{10,11} In addition, these signals move further downfield as the temperature is lowered, showing

positive slopes in Curie plots. As given in Figures S1 and S2 of the Supporting Information, $[\text{Fe}(\text{T}^n\text{PrP})(\text{L})_2]\text{X}$ and $[\text{Fe}(\text{T}^c\text{PrP})(\text{L})_2]\text{X}$ with $\text{L} = 4\text{-CNPY}, \text{Py},$ and 3-MePy fall into this category. Thus, these complexes are expected to have the $(d_{xz}, d_{yz})^4(d_{xy})^1$ ground state. In contrast, $[\text{Fe}(\text{T}^n\text{PrP})(\text{L})_2]\text{X}$ and $[\text{Fe}(\text{T}^c\text{PrP})(\text{L})_2]\text{X}$ with $\text{L} = \text{HIm}, 4\text{-Me}_2\text{NPy},$ and 2-MeIm showed the upfield shifted pyrrole signals together with the negative slopes in Curie plots. Thus, these complexes are expected to adopt the $(d_{xy})^2(d_{xz}, d_{yz})^3$ ground state. $[\text{Fe}(\text{T}^n\text{PrP})(\text{CN})_2]^-$ is a borderline case because the pyrrole signal appeared near 0 ppm at 25 °C in addition to the small negative slope in Curie plots. In the case of the isopropyl complexes, $[\text{Fe}(\text{T}^i\text{PrP})(\text{L})_2]\text{X}$, both the chemical shifts in Table 1 and the Curie plots in Figure S3 clearly indicate that all the complexes have the $(d_{xz}, d_{yz})^4(d_{xy})^1$ ground state.

¹³C NMR chemical shift of the meso carbons is also a good probe to determine the ground state.^{11,30} As mentioned, one of the reasons for some low-spin iron(III) porphyrin complexes to have the unusual ground state with $(d_{xz}, d_{yz})^4(d_{xy})^1$ electron configuration is the S_4 -ruffling of the porphyrin core. The deformation of this mode makes the interaction between the singly occupied iron d_{xy} and porphyrin a_{2u} orbital possible.^{3,10} Since the porphyrin a_{2u} orbital has the large electron densities on the meso carbon atoms,^{31,32} the interaction would cause large downfield shifts for these carbon signals.¹¹ The data in Table 2 indicate that the ground state of the complexes determined by the ¹H NMR chemical shifts is consistent with the ¹³C NMR results. That is, the meso carbon signals in $[\text{Fe}(\text{T}^n\text{PrP})(\text{L})_2]^+$ and $[\text{Fe}(\text{T}^c\text{PrP})(\text{L})_2]^+$ with $\text{L} = 4\text{-CNPY}, \text{Py}, 3\text{-MePy},$ and CN^- appeared fairly downfield, $\delta > 300$ ppm. In contrast, the complexes with $\text{L} = \text{HIm}, 4\text{-Me}_2\text{NPy},$ and 2-MeIm showed the corresponding signals at $\delta < 200$ ppm. Although the ground state of $[\text{Fe}(\text{T}^n\text{PrP})(\text{CN})_2]^-$ was ambiguous in the ¹H NMR spectra, the ¹³C NMR result strongly suggests that the complex has the $(d_{xz}, d_{yz})^4(d_{xy})^1$ ground state; the meso signal appeared at 286 ppm at 25 °C and moved downfield as the temperature was lowered. In the case of $[\text{Fe}(\text{T}^i\text{PrP})(\text{L})_2]^+$, all the complexes showed the meso carbon signals at $\delta > 300$ ppm, supporting that these complexes have the $(d_{xz}, d_{yz})^4(d_{xy})^1$ ground state. It is noteworthy that the meso carbon signal of $[\text{Fe}(\text{T}^i\text{PrP})(4\text{-CNPY})_2]^+$ appeared extremely downfield, 918 ppm at -50 °C, suggesting that a considerable amount of spin exists at these carbon atoms. Quantitative treatment of the spin densities at the carbon and nitrogen atoms of this complex will be discussed later in this paper.

Conclusive evidence on the electronic ground state can be obtained from the EPR g values. While the complexes with the $(d_{xz}, d_{yz})^4(d_{xy})^1$ ground state exhibit the axial type spectra,^{1-4,7,10,11} those with the $(d_{xy})^2(d_{xz}, d_{yz})^3$ ground state show either the rhombic or the large g_{max} type EPR spectra.²⁶⁻²⁸ On the basis of the ¹H NMR, ¹³C NMR, and EPR spectra, the electronic ground state of all the complexes examined in this study is determined as listed in Table 3. It should be noted that the EPR method examined in this study determines the electronic ground state of the low-spin iron(III) complexes at 4.2 K. Thus, at higher temperature where the NMR spectra are taken, the ground-state electron configuration could be different. However, all the complexes with positive Curie slopes of the meso carbon signals exhibited the axial type EPR spectra; all the complexes with negative Curie slopes showed either rhombic or large g_{max} type

(30) Nakamura, M.; Nakamura, N. *Chem. Lett.* **1991**, 1885-1888.

(31) Fajer, J.; Borg, D. C.; Forman, A.; Felton, R. H.; Vegh, L.; Dolphin, D. *Ann. N. Y. Acad. Sci.* **1973**, *206*, 349-364.

(32) Fajer, J.; Davis, M. S. In *The Porphyrins*; Dolphin D., Ed.; Academic Press: New York, 1979; Vol. IV, pp 197-256.

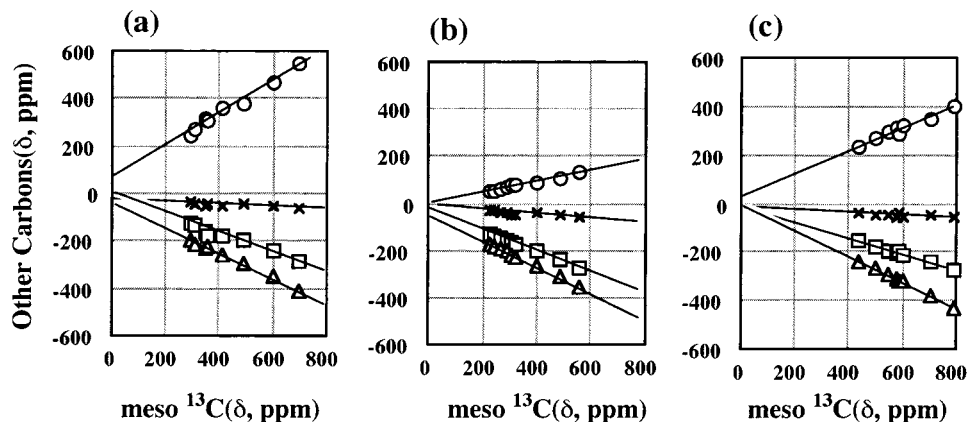


Figure 4. Correlation of the isotropic shifts between the meso-carbon and other carbons in (a) $[\text{Fe}(\text{T}^n\text{PrP})(\text{L})_2]^+$, (b) $[\text{Fe}(\text{T}^c\text{PrP})(\text{L})_2]^+$, and (c) $[\text{Fe}(\text{T}^i\text{PrP})(\text{L})_2]^+$ where L is 4-CNPy, Py, or 3-MePy: \square , α -carbons (C_α) of the meso alkyl substituents; \circ , β -carbons (C_β) of the meso alkyl substituents; \triangle , α -pyrrole carbons (py- α); \times , β -pyrrole carbons (py- β).

EPR spectra. Thus, the NMR measurement, especially the variable-temperature measurement of the ^{13}C NMR spectra, is a good method to determine the electronic ground state at higher temperature.

The contribution of the $(d_{xz}, d_{yz})^4(d_{xy})^1$ state to the electronic ground state differs from complex to complex; it increases if the energy level of the iron d_{xy} orbital is raised relative to those of the d_π orbitals. The EPR g values in Table 3 indicate that the energy difference between the d_{xy} and d_π orbitals, $E(d_{xy}) - E(d_\pi)$, among pyridine complexes increases in the following order at 4.2 K: $[\text{Fe}(\text{T}^i\text{PrP})(4\text{-NMe}_2\text{Py})_2]^+ < [\text{Fe}(\text{T}^i\text{PrP})(\text{Py})_2]^+ < [\text{Fe}(\text{T}^i\text{PrP})(4\text{-CNPy})_2]^+$. In the case of $[\text{Fe}(\text{T}^i\text{PrP})(4\text{-CNPy})_2]^+$, which shows the purest $(d_{xz}, d_{yz})^4(d_{xy})^1$ ground state among the complexes examined in this study, the energy difference reaches as much as 4.3λ in units of the spin-orbit coupling constant (λ).^{27,33,34} Corresponding to the EPR results, the meso- ^{13}C chemical shifts increased from 402.2 ppm in $[\text{Fe}(\text{T}^i\text{PrP})(4\text{-NMe}_2\text{Py})_2]^+$ to 917.5 ppm in $[\text{Fe}(\text{T}^i\text{PrP})(4\text{-CNPy})_2]^+$ at -50°C .

^{13}C NMR Characteristics in $(d_{xz}, d_{yz})^4(d_{xy})^1$ Type Complexes. As mentioned, one of the characteristic features in the ^{13}C NMR spectra of the complexes with the $(d_{xz}, d_{yz})^4(d_{xy})^1$ ground state is the presence of downfield shifted meso carbon signals; the meso carbon signal moves downfield as the contribution of the $(d_{xz}, d_{yz})^4(d_{xy})^1$ state increases.^{11,30} To determine which carbons are sensitive to the electron configuration, we have plotted the isotropic shifts of the α - and β -pyrrole ring carbons and those of the substituent at various temperatures against those of the meso carbons of the same complex. Panels a–c in Figure 4 show such plots for $[\text{Fe}(\text{T}^n\text{PrP})(\text{L})_2]^+$, $[\text{Fe}(\text{T}^c\text{PrP})(\text{L})_2]^+$, and $[\text{Fe}(\text{T}^i\text{PrP})(\text{L})_2]^+$, respectively, where L's are 4-CNPy, Py, and 3-MePy; all of these complexes have the less common ground state with $(d_{xz}, d_{yz})^4(d_{xy})^1$ electron configuration. Good linear lines with $R^2 = 0.965$ to 0.997 were obtained for the py- α , C_α , and C_β carbons, suggesting that the chemical shifts of these carbon atoms also reflect the electron configuration of the iron(III) ions. The slopes of the py- α carbons were quite similar in the ^nPr , ^cPr , and ^iPr complexes, -0.51 , -0.57 , and -0.56 , respectively. The slopes of the C_α carbons were also quite similar among three types of complexes, -0.37 , -0.44 , and -0.34 , respectively. The results indicate that the chemical shifts of these carbons are mainly determined by the contribution of the $(d_{xz}, d_{yz})^4(d_{xy})^1$ state to the electronic ground state of the complex. Thus, not only the meso but also the py- α and C_α carbon shifts can be good probes to determine the ground state.

It should be noted, however, that the absolute values of the slopes are smaller than 1.0, suggesting that the meso carbon shift is more sensitive to the change in ground state than the py- α and C_α shifts. In contrast, the isotropic shifts of the py- β carbon were observed in a narrow range, 54.7 – 89.7 ppm at -50°C , despite the large difference in the isotropic shifts of the meso carbon; the slopes of the Curie plots are in the range -0.02 to -0.06 . Thus, the py- β carbon shift cannot be a probe to determine the ground state.

While the slopes of the py- α and C_α showed only a small difference among three types of complexes, those of the C_β differed to a great extent: $+0.69$, $+0.23$, and $+0.45$ for the ^nPr , ^cPr , and ^iPr complexes, respectively. The results suggest that the isotropic shifts of the C_β carbons are different among three types of complexes even if those of the meso carbons are the same. The large difference in slopes can be ascribed to the conformation of the meso alkyl groups. The Karplus equation suggests that the hyperfine coupling constant of the C_β carbon increases as the dihedral angle between p_z - $C_{\text{meso}}-C_\alpha$ and $C_{\text{meso}}-C_\alpha-C_\beta$ decreases, where p_z is the p orbital at the meso carbon having an unpaired electron.³⁵ Thus, the largest slope observed in $[\text{Fe}(\text{T}^n\text{PrP})(\text{L})_2]^+$ can be explained in terms of the smaller dihedral angle in this type of complex as compared with those in the other two types of complexes; the average dihedral angles in high-spin $[\text{Fe}(\text{T}^n\text{PrP})\text{Cl}]$ and $[\text{Fe}(\text{T}^i\text{PrP})\text{Cl}]$ have been determined to be 1.4° and 25.0° , respectively, by X-ray crystallographic analysis.^{36,37} The conformation effect of the meso alkyl groups on the chemical shifts is also clearly shown in the ^1H NMR spectra. Figure 5 demonstrates the isotropic shifts of the H_α protons of the three types of complexes plotted against those of the corresponding meso carbons. The slopes are very much different among the three types of complexes: $+0.11$, $+0.31$, and $+0.043$ for $[\text{Fe}(\text{T}^n\text{PrP})(\text{L})_2]^+$, $[\text{Fe}(\text{T}^c\text{PrP})(\text{L})_2]^+$, and $[\text{Fe}(\text{T}^i\text{PrP})(\text{L})_2]^+$, respectively. The result indicates that the dihedral angles between p_z - $C_{\text{meso}}-C_\alpha$ and $C_{\text{meso}}-C_\alpha-H$ are in the following order: $[\text{Fe}(\text{T}^c\text{PrP})(\text{L})_2]^+ < [\text{Fe}(\text{T}^n\text{PrP})(\text{L})_2]^+ < [\text{Fe}(\text{T}^i\text{PrP})(\text{L})_2]^+$.¹² The average dihedral angle in $[\text{Fe}(\text{T}^c\text{PrP})(\text{L})_2]^+$ is expected to be very small because the X-ray crystallographic analysis of analogous $[\text{Fe}(\text{TMCP})\text{Cl}]$ has shown the average dihedral angle to be 4.1° as reported by Marchon, Latos-Grazynski, Scheidt, and co-workers.^{38,39}

(35) Karplus, M. *J. Am. Chem. Soc.* **1963**, *85*, 2870–2871.

(36) Ohgo, Y.; Ikeue, T.; Nakamura, M. *Acta Crystallogr., Sect. C* **1999**, *1817*–1819.

(37) Ikeue, T.; Ohgo, Y.; Uchida, A.; Nakamura, M.; Fujii, H.; Yokoyama, M. *Inorg. Chem.* **1999**, *38*, 1276–1281.

(33) Taylor, C. P. S. *Biochim. Biophys. Acta* **1977**, *491*, 137–149.

(34) Bohan, T. L. *J. Magn. Reson.* **1977**, *26*, 109–118.

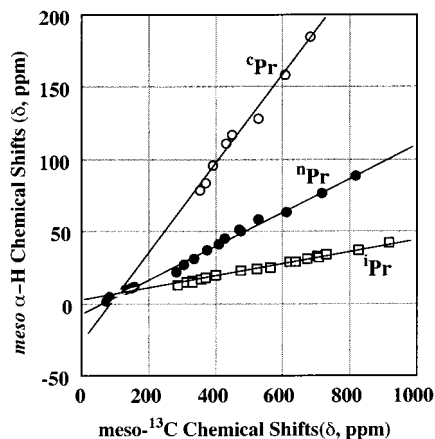


Figure 5. Correlation of the isotropic shifts between the meso- ^{13}C and meso-H $_{\alpha}$.

Spin Densities at Porphyrin Carbon and Nitrogen Atoms.

Spin distribution of the low-spin iron(III) porphyrin complexes with the common $(d_{xy})^2(d_{xz}, d_{yz})^3$ ground state has been extensively studied.^{17–20} Since we have been able to assign all the proton and carbon signals in the complexes with the less common $(d_{xz}, d_{yz})^4(d_{xy})^1$ ground state, it is now possible to determine the spin distribution at the porphyrin core sites in these complexes. Determination of the spin distribution was carried out by the method developed by Wüthrich, La Mar, Goff, Turner, Mispelter, and others.^{17–20,40–44}

(i) ^1H NMR Spectra. The isotropic shift (δ_{iso}) of a paramagnetic molecule consists of a contact shift (δ_{con}) and a dipolar shift (δ_{dip}). The metal-centered dipolar shift in the complexes with axial symmetry is defined by eq 1 where χ values are molecular susceptibilities and the term $(3 \cos^2\theta - 1)/r^3$ is referred to as the axial geometric factor:

$$\delta_{\text{dip}}^{\text{MC}} = (1/12\pi)(\chi_{\parallel} - \chi_{\perp})(3 \cos^2\theta - 1)/r^3 \quad (1)$$

On the assumption that the spin multiplet ground state with effective spin S is well isolated from the excited electronic state, and that the second-order Zeeman (SOZ) interaction is negligible, eq 1 can be simplified to

$$\delta_{\text{dip}}^{\text{MC}} = (\mu_0/4\pi)[\mu_B^2 S(S+1)/9kT](g_{\parallel}^2 - g_{\perp}^2)(3 \cos^2\theta - 1)/r^3 \quad (2)$$

where μ_0 and μ_B represent the permeability of vacuum and the electron Bohr magneton, respectively.^{1,20,45} It should be noted that eq 2 is a rough approximation since the SOZ contribution

(38) Mazzanti, M.; Marchon, J.-C.; Wojaczynski, J.; Wolowicz, S.; Latso-Grazynski, L.; Shang, M.; Scheidt, W. R. *Inorg. Chem.* **1998**, *37*, 2476–2481.

(39) Jentzen, W.; Simpson, M. C.; Hobbs, J. D.; Song, X.; Ema, T.; Nelson, N. Y.; Medforth, C. J.; Smith, K. M.; Veyrat, M.; Mazzanti, M.; Ramasseul, R.; Marchon, J. C.; Takeuchi, T.; Goddard, W. A., III; Shelnutt, J. A. *J. Am. Chem. Soc.* **1995**, *117*, 11085–11097.

(40) La Mar, G. N.; Walker, F. A. In *The Porphyrins*; Dolphin D., Ed.; Academic Press: New York, 1979; Vol. IV, pp 61–157.

(41) Goff, H. In *Iron Porphyrin*; Lever, A. B. P., Gray, H. B., Eds.; Physical Bioinorganic Chemistry Series 1; Addison-Wesley: Reading, MA, 1983; Part I, pp 237–281.

(42) Bertini, I.; Luchinat, C. In *NMR of Paramagnetic Molecules in Biological Systems*; Lever, A. B. P., Gray, H. B., Eds.; Physical Bioinorganic Chemistry Series 3; The Benjamin/Cummings: Menlo Park, CA, 1986; pp 165–229.

(43) Turner, P.; Gunter, M. J. *Inorg. Chem.* **1994**, *33*, 1406–1415.

(44) Mispelter, J.; Momenteau, M.; Lhoste, J.-M. Heteronuclear Magnetic Resonance. In *NMR of Paramagnetic Molecules*; Berliner, L. J., Reuben, J., Eds.; Plenum Press: New York, 1993; Biological Magnetic Resonance, Vol. 12, pp 299–355.

to the magnetic susceptibilities of heme systems is not negligible.^{1,20} If the dipolar shift of a proton $\delta_{\text{dip}}(\text{A})$ in complex **A**, its geometric factor $\{(3 \cos^2\theta - 1)/r^3\}_{\text{A}}$, and the EPR g values of the complex are known, we can obtain the dipolar shift $\delta_{\text{dip}}(\text{B})$ of a proton in the other low-spin complex **B** from

$$\delta_{\text{dip}}^{\text{MC}}(\text{B}) = [(g_{\parallel}^2 - g_{\perp}^2)_{\text{B}}/(g_{\parallel}^2 - g_{\perp}^2)_{\text{A}}]\{[(3 \cos^2\theta - 1)/r^3]_{\text{B}}/\{(3 \cos^2\theta - 1)/r^3\}_{\text{A}}\}\delta_{\text{dip}}^{\text{MC}}(\text{A}) \quad (3)$$

The contact shift is then obtained by $\delta_{\text{con}} = \delta_{\text{iso}} - \delta_{\text{dip}}$. Once the contact shift is determined, the proton hyperfine coupling constant, A^{H} , can be calculated by

$$\delta_{\text{con}} = (A^{\text{H}})\{2\pi g\mu_B S(S+1)\}/(3\gamma_{\text{H}}\hbar kT) \quad (4)$$

where $g = [(g_{xx}^2 + g_{yy}^2 + g_{zz}^2)/3]^{1/2}$. Because the proton hyperfine coupling constant is proportional to the spin density ρ^{π} of the carbon atom to which the proton is attached, it is possible to determine the spin density at the carbon by

$$A^{\text{H}}/h = (Q_{\text{CH}}^{\text{H}}\rho^{\pi})/2S \quad (5)$$

where Q_{CH}^{H} is a proportional constant.^{46,47}

The spin densities of the porphyrin carbon and nitrogen atoms in $[\text{Fe}(\text{T}^{\text{i}}\text{PrP})(4\text{-CNPy})_2]^+$ have been examined, because this complex has the purest $(d_{xz}, d_{yz})^4(d_{xy})^1$ ground state among the complexes examined in this study as is revealed from the most downfield shifted pyrrole proton and meso carbon signals together with the smallest EPR g_{\perp} value. The δ_{iso} values for the isopropyl CH and pyrrole-H were determined to be 26.8 and 4.20 ppm at 25 °C on the basis of the corresponding chemical shifts in diamagnetic $[\text{Co}(\text{T}^{\text{i}}\text{PrP})(\text{HIm})_2]\text{Cl}$.⁴⁸ Curie plots of these signals gave good linear lines, which were extrapolated close to the origin. For the determination of the $\delta_{\text{dip}}^{\text{MC}}$ values from eq 3, well-characterized $[\text{Fe}(\text{T}^{\text{n}}\text{PrP})(\text{HIm})_2]^+$ was selected as a reference complex.⁴⁵ The ratio $(g_{\parallel}^2 - g_{\perp}^2)_{\text{B}}/(g_{\parallel}^2 - g_{\perp}^2)_{\text{A}}$ was calculated to be -0.566 from the g values listed in Table 3. The ratios in the geometric factors, $\{(3 \cos^2\theta - 1)/r^3\}_{\text{B}}/\{(3 \cos^2\theta - 1)/r^3\}_{\text{A}}$, were determined to be 1.11 and 1.12 for the isopropyl CH and pyrrole-H, respectively, on the basis of the X-ray molecular structure of strongly S_4 -ruffled $[\text{Fe}(\text{T}^{\text{i}}\text{PrP})(\text{THF})_2]\text{ClO}_4$.⁴⁹ The $\delta_{\text{dip}}^{\text{MC}}$ values for the isopropyl CH and pyrrole-H were calculated to be 2.8 and 3.7 ppm, respectively. Thus, the contact shifts of these protons were determined to be 24.0 and 0.50 ppm, respectively. The proton hyperfine coupling constants, A^{H}/h , for the isopropyl CH and pyrrole-H were calculated from eq 4 to be 0.813 and 0.017 MHz, respectively, at 25 °C. The π spin density at the β -pyrrole carbon was estimated to be -0.00026 by the use of $Q_{\text{CH}}^{\text{H}} = -65.8$ MHz in eq 5.^{45,50} In principle, the π spin density at the meso carbon can be determined from the hyperfine coupling constant of the isopropyl CH. However, the hyperfine coupling constant has angular dependence as given below:

$$A^{\text{H}}/h = (B_0 + B_2 \cos^2\theta)\rho^{\pi} \quad (6)$$

where θ is the dihedral angle between $p_z\text{-C}_{\text{meso}}\text{-C}_{\alpha}$ and $\text{C}_{\text{meso}}\text{-}$

(45) Bertini, I.; Luchinat, C. In *NMR of Paramagnetic Substances*; Lever, A. B. P., Ed.; Coordination Chemistry Reviews 150; Elsevier: Amsterdam, 1996; pp 29–75.

(46) Heller, C.; McConnell, H. M. *J. Chem. Phys.* **1960**, *32*, 1535

(47) McLachlan, A. D. *Mol. Phys.* **1958**, *1*, 233–240.

(48) Saitoh, T.; Ikeue, T.; Ohgo, Y.; Nakamura, M. *Tetrahedron* **1997**, *53*, 12487–12496.

(49) Ohgo, Y.; Saitoh, T.; Nakamura, M. To be submitted for publication.

(50) Karplus, M.; Fraenkel, G. K. *J. Chem. Phys.* **1961**, *35*, 1312–1323.

C_{α} -H. Usually, B_0 is negligible in comparison with B_2 and B_2 is estimated to be 140 MHz.^{45,47,51} Thus, the spin density at the meso carbon is presented as

$$\rho_{\text{meso}}^{\pi} = 0.813/(140 \cos^2 \theta) \quad (7)$$

If the dihedral angle θ is 72° as in the case of $[\text{Fe}(\text{T}^i\text{PrP})(\text{THF})_2]\text{ClO}_4$,⁴⁹ the π spin density is calculated to be 0.061 from the equation.

(ii) **¹³C NMR Spectra.** The carbon-13 isotropic shift is presented by

$$\delta_{\text{iso}} = \delta_{\text{dip}}^{\text{MC}} + \delta_{\text{dip}}^{\text{LC}} + \delta_{\text{con}} \quad (8)$$

where $\delta_{\text{dip}}^{\text{LC}}$ is a ligand centered dipolar shift.^{40–44} Carbon contact shifts originate from unpairing of carbon 1s electrons and unpairing of the three carbon sp^2 bonding pairs. Thus, the contact shift for the β -pyrrole carbon can be written by the Karplus and Frankel equation

$$\delta_{\text{con}}(\text{py}-\beta) = [(S^C + 2Q_{\text{CC}'}^C + Q_{\text{CH}}^C)\rho_{\beta}^{\pi} + Q_{\text{C}'\text{C}}^C(\rho_{\beta}^{\pi} + \rho_{\alpha}^{\pi})]F^C$$

where $F^C = \{2\pi g_{\text{uB}} S(S+1)\}/(3\gamma_{\text{C}} kT)$.^{50,52}

In the equation, the S^C term indicates polarization of the 1s orbital. The $Q_{\text{CC}'}^C$ and Q_{CH}^C terms reflect polarization of the three sp^2 bonds by π -spin density at the observed carbon atom. The $Q_{\text{C}'\text{C}}^C$ term represents polarization of the C–C bond by π spin densities centered on the neighboring carbon atoms. The $\delta_{\text{dip}}^{\text{LC}}$ is assumed to be proportional to the spin density ρ^{π} at the observed carbon atom and is given by $\delta_{\text{dip}}^{\text{LC}} = D\rho^{\pi}$.

Thus, the $(\delta_{\text{dip}}^{\text{LC}} + \delta_{\text{con}})$ values for the $\text{py}-\alpha$, $\text{py}-\beta$, and meso carbons, which can easily be obtained by the subtraction of the $\delta_{\text{dip}}^{\text{MC}}$ term from δ_{iso} , are expressed by eqs 9, 10, and 11, respectively.

For $\text{py}-\alpha$:

$$\delta_{\text{con}} + \delta_{\text{dip}}^{\text{LC}} = D\rho_{\text{py}-\alpha}^{\pi} + [(S^C + 2Q_{\text{CC}'}^C + Q_{\text{CN}}^C)\rho_{\text{py}-\alpha}^{\pi} + Q_{\text{C}'\text{C}}^C(\rho_{\text{py}-\beta}^{\pi} + \rho_{\text{meso}}^{\pi}) + Q_{\text{NC}}^C\rho_{\text{N}}^{\pi}] \cdot F^C \quad (9)$$

For $\text{py}-\beta$:

$$\delta_{\text{con}} + \delta_{\text{dip}}^{\text{LC}} = D\rho_{\text{py}-\beta}^{\pi} + [(S^C + 2Q_{\text{CC}'}^C + Q_{\text{CH}}^C)\rho_{\text{py}-\beta}^{\pi} + Q_{\text{C}'\text{C}}^C(\rho_{\text{py}-\beta}^{\pi} + \rho_{\text{py}-\alpha}^{\pi})] \cdot F^C \quad (10)$$

For meso:

$$\delta_{\text{con}} + \delta_{\text{dip}}^{\text{LC}} = D\rho_{\text{meso}}^{\pi} + [(S^C + 3Q_{\text{CC}'}^C)\rho_{\text{meso}}^{\pi} + 2Q_{\text{C}'\text{C}}^C\rho_{\text{py}-\alpha}^{\pi}] \cdot F^C \quad (11)$$

The π spin density at the isopropyl methine carbon (C_{α}) is supposed to be 0. Thus, the spin density at the meso carbon can be obtained from the contact shift value of the methine carbon by

$$\delta_{\text{con}}(C_{\alpha}) = Q_{\text{C}'\text{C}}^C\rho_{\text{meso}}^{\pi}F^C \quad (12)$$

The S^C and Q^C values are as follows; $S^C = -35.5$ MHz; $Q_{\text{CC}'}^C = +40.3$ MHz; $Q_{\text{CH}}^C = +54.6$ MHz; $Q_{\text{CN}}^C = +40.3$ MHz; $Q_{\text{C}'\text{C}}^C = -39.0$ MHz; and $Q_{\text{NC}}^C = -39.0$ MHz.⁵⁰ In the case

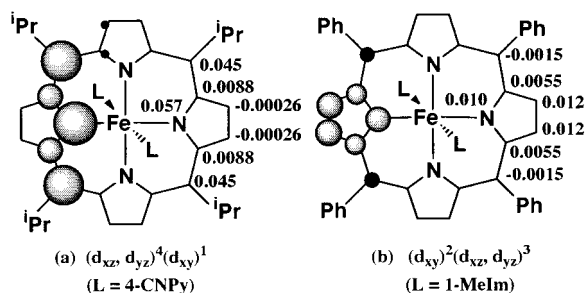


Figure 6. Spin distribution of low-spin ferric porphyrin complexes with different electron configuration: (a) $[\text{Fe}(\text{T}^i\text{PrP})(4\text{-CNPY})_2]^+$ with $(d_{xz}, d_{yz})^4(d_{xy})^1$ ground state and (b) $[\text{Fe}(\text{TPP})(1\text{-MeIm})_2]^+$ with $(d_{xy})^2(d_{xz}, d_{yz})^3$ ground state reported by Goff.²⁰ Spin density at each carbon and nitrogen is presented by the volume of a sphere.

of $[\text{Fe}(\text{T}^i\text{PrP})(4\text{-CNPY})_2]^+$, the π spin density at the meso carbons, ρ_{meso}^{π} , was calculated to be 0.045 from eq 12. By putting the ρ_{meso}^{π} value into eq 7, we can estimate the dihedral angle θ to be 69° , which is ca. 3° smaller than the corresponding dihedral angle in $[\text{Fe}(\text{T}^i\text{PrP})(\text{THF})_2]\text{ClO}_4$. Solution of the simultaneous eqs 9–11 using $\rho_{\text{meso}}^{\pi} = 0.045$ and $\rho_{\text{py}-\beta}^{\pi} = -0.00026$ yields ρ_{α}^{π} , ρ_{N}^{π} , and D values of 0.0088, 0.057, and 4516 ppm, respectively. Figure 6a shows the spin densities at the carbon and nitrogen atoms in $[\text{Fe}(\text{T}^i\text{PrP})(4\text{-CNPY})_2]^+$. For comparison, the spin densities in $[\text{Fe}(\text{TPP})(1\text{-MeIm})_2]^+$ determined by Goff are also shown in Figure 6b).²⁰ Figure 6 indicates that the major spin densities in $[\text{Fe}(\text{T}^i\text{PrP})(4\text{-CNPY})_2]^+$ are at the pyrrole nitrogen and meso carbon atoms. In contrast, the major spin densities in $[\text{Fe}(\text{TPP})(1\text{-MeIm})_2]^+$ are at the $\text{py}-\beta$ carbon atoms.²⁰ Thus, the large downfield shift of the meso carbon in $[\text{Fe}(\text{T}^i\text{PrP})(4\text{-CNPY})_2]^+$, $\delta_{\text{iso}} = 583.7$ ppm at 25°C , is ascribed to the large spin densities at these carbon atoms. It seems to be unusual that the α -pyrrole carbon atom has positive spin density $\rho_{\pi} = 0.0088$, though the contact shift term shows a fairly large negative value $\delta_{\text{con}} = -377$ ppm. The large negative contact shift can be explained in terms of the spin polarization from the neighboring pyrrole nitrogen and meso carbon atoms; these atoms have large spin densities, 0.057 and 0.045, respectively. Table 4 lists the individual contributions to the observed isotropic shifts. In the case of the α -pyrrole carbon atoms, the spin density of 0.0088 induces the downfield shift of 127 ppm, which is obtained by the summation of the S^C , $\sum Q_{\text{CX}}^C$, and $\delta_{\text{dip}}^{\text{LC}}$ terms. However, the major contribution to the isotropic shift of the α -pyrrole carbon atoms comes from the $\sum Q_{\text{XC}}^C$ term, -464 ppm, indicating that the spin polarization from the neighboring atoms is the major reason for the upfield shift. The observation is not unprecedented. Turner and Gunter reported the π spin densities at porphyrin core sites in $[\text{Mn}(\text{TPP})]\text{ClO}_4$ on the basis of the ¹³C NMR analysis.⁴³ Although the β -pyrrole signal appears at -204 ppm, the spin density at the β -pyrrole carbon is estimated to be $+0.014$. The large upfield shift of the β -pyrrole carbon is explained in terms of the large spin density of the adjacent α -pyrrole carbon which is 0.063. It should be noted that the total spin densities on the porphyrin ring in $[\text{Fe}(\text{T}^i\text{PrP})(4\text{-CNPY})_2]^+$ are as much as 0.48 electron per porphyrin, suggesting the radical character of this complex. This contrasts to the corresponding value in $[\text{Fe}(\text{T}^i\text{PrP})(1\text{-MeIm})_2]^+$ which has only 0.17 electron.²⁰

Conclusion

¹H and ¹³C NMR measurements of 21 low-spin (meso-tetraalkylporphyrinato)iron(III) complexes at various temperatures have revealed that the spectral characteristics of the complexes with the less common $(d_{xz}, d_{yz})^4(d_{xy})^1$ ground state

(51) Stone, E. W.; Maki, A. H. *J. Chem. Phys.* **1962**, *37*, 1326–1333.

(52) Strom, E. T.; Underwood, G. R.; Jurkowitz, D. *Mol. Phys.* **1972**, *24*, 901–904.

Table 4. Comparison of ^{13}C NMR Contact and Dipolar Shifts between $[\text{Fe}(\text{T}^i\text{PrP})(4\text{-CNPY})_2]\text{ClO}_4(\text{A})^a$ and $[\text{Fe}(\text{TPP})(1\text{-MeIm})_2]\text{Cl}(\text{B})^b$ at 25 $^\circ\text{C}$

complexes	nuclei	δ_{iso}	δ_{dip}			contribution to δ_{con}		
			$\delta_{\text{dip}}^{\text{MC}}$	$\delta_{\text{dip}}^{\text{LC}}$	δ_{con}	S_{C}	$\Sigma Q_{\text{CX}}^{\text{C}}$	$\Sigma Q_{\text{XC}}^{\text{C}}$
A ($D = 4516$)	meso	583.7	11.6	203.2	369	-187	636	-80
	C_α	-201.3	3.6	—	-205	—	—	-205
	Py- α	-319.6	17.9	39.7	-377	-37	124	-464
	Py- β	-36.5	6.6	-1.0	-42	1	-4	-39
B ($D = 6567$)	meso	-73.2	-22	10	-61	5	-20	-45
	Py- α	-101.5	-31	-36	-34	-21	70	-83
	Py- β	-36.0	-11	-78	53	-44	168	-71

^a This work. ^b Data at 26 $^\circ\text{C}$ reported by Goff.²⁰

are (i) downfield shifted pyrrole-H and meso- H_α signals in ^1H NMR spectra,^{1-4,6,7,9-15} (ii) downfield shifted meso and meso- C_β signals in ^{13}C NMR spectra,^{11,30} and (iii) upfield shifted meso- C_α and α -pyrrole signals in ^{13}C NMR spectra. In contrast, β -pyrrole carbon signals have appeared in a narrow range, 55 to 90 ppm at -50 $^\circ\text{C}$. Both the ^1H and ^{13}C NMR spectra of these complexes have indicated that the contribution of the $(d_{xz}, d_{yz})^4(d_{xy})^1$ state to the electronic ground state increases in the following order: $\text{HIm} < 4\text{-Me}_2\text{NPy} < 2\text{-MeIm} < \text{CN}^- < 3\text{-MePy} < \text{Py} < 4\text{-CNPY}$. Analysis of the ^1H and ^{13}C NMR isotropic shifts of $[\text{Fe}(\text{T}^i\text{PrP})(4\text{-CNPY})_2]^+$ using the Karplus-Frankel equation has yielded the spin densities at porphyrin carbon and nitrogen atoms. The major spin densities are at the pyrrole nitrogen (5.7%) and meso carbon (4.5%) atoms. Thus, the large downfield shifts of the meso and meso C_β signals as well as the large upfield shift of the meso C_α signals are ascribed to the considerable amount of spin densities at the meso carbon atoms. The large upfield shift of the α -pyrrole carbon signals, which is commonly observed in the $(d_{xz}, d_{yz})^4(d_{xy})^1$ type complexes, can be explained in terms of the spin polarization from the neighboring nitrogen and meso carbon atoms. Thus, the spin

distribution in the $(d_{xz}, d_{yz})^4(d_{xy})^1$ type complexes is quite different from that in the $(d_{xy})^2(d_{xz}, d_{yz})^3$ type complexes which have the major spin density at the β -pyrrole carbon atoms.¹⁷⁻²⁰ The total spin delocalized onto the porphyrin ring is 0.48 unpaired electron in $[\text{Fe}(\text{T}^i\text{PrP})(4\text{-CNPY})_2]^+$, which is much larger than the corresponding value, 0.17, in $[\text{Fe}(\text{TPP})(1\text{-MeIm})_2]^+$.²⁰

Acknowledgment. This work was supported by a Grant in Aid for Scientific Research (No. 10640551) from the Ministry of Education, Science, Culture and Sports of Japan and by the Joint Studies Program (1998-1999) of the Institute for Molecular Science.

Supporting Information Available: Tables of ^1H and ^{13}C NMR chemical shift at various temperature, Curie plots of the pyrrole protons, and COSY spectrum of $[\text{Fe}(\text{T}^i\text{PrP})(2\text{-MeIm})_2]\text{-Cl}$ (PDF). This material is available free of charge via the Internet at <http://pubs.acs.org>.

JA992219N